CrossMark

Corrosion Inhibition Performance of the Synergistic Effect of *Rosmarinus officinalis* and 5-Bromovanillin on 1018 Carbon Steel in Dilute Acid Media

Roland Tolulope Loto

Abstract The corrosion inhibition effect of environmentally friendly organic admixture of *Rosmarinus officinalis* and 5-bromovanillin on 1018 carbon steel in 1 M HCl and H_2SO_4 solution was assessed through potentiodynamic polarization, coupon measurement, optical microscopy and ATF-FTIR spectroscopy. Experimental data show that the compound performed more effectively in HCl solution with maximum inhibition efficiency 92.57 and 94% in comparison with 64.57 and 64.55% in H_2SO_4 from electrochemical analysis due to film formation and chemisorption adsorption of the compound. Functional groups of amines, amides, H–bonded alcohols and phenols, C–H stretch alkanes, alkynes and C–C stretch in-ring aromatics identified through ATF-FTIR spectroscopy completely adsorbed on the steel surface in HCl, but partially in H_2SO_4 as shown in the decreased peak intensity. Thermodynamic calculations showed the cationic adsorption to be through chemisorption and physiochemical mechanism according to Langmuir, Freundlich and Temkin adsorption isotherms. Images from optical microscopy showed a well-protected surface morphology of the inhibited steel in comparison with images from the corroded stainless steel. Severe surface deterioration and macropits were observed in the uninhibited samples. The inhibition property of the organic compound was determined to be mixed type.

Keywords Corrosion · Inhibitor · *Rosmarinus officinalis* · Vanillin · Acid

R. T. Loto (✉)
Department of Mechanical Engineering, Covenant University, Ota, Ogun State, Nigeria
e-mail: tolu.loto@gmail.com

Introduction

Molecules of natural or organic origin exhibiting a strong affinity for metallic surfaces are the focus of research toward the development of environmentally tolerant corrosion inhibiting compounds. Among the green corrosion inhibitors are organic compounds that act by adsorption on the metal surface, such as ascorbic acid [1–5]. In acidic industrial environments, compounds containing heteroatoms, aldehydes and some alkaloids such as papaverine and nicotine are used as inhibitors. Inorganic chemical compounds such as chromate, nitrates and phosphates are the most common corrosion inhibitors for metallic alloys in aqueous systems; however, of recent these compounds have been facing more stringent regulations on their use by the US Environmental Protection Agency and other governing agencies worldwide due to their adverse environmental and health effects. In view concerns, development and use of corrosion inhibitors based on low molecular weight compounds of organic origin have proven to be successful carbon steels, but most tend to be efficient inhibitors at relatively high concentrations. Previous research has shown *Rosmarinus officinalis* to be very promising in the development and use of safe compounds for corrosion inhibition. The main chemical components of rosemary include borneol, bornyl acetate, camphor, cineole, camphene, catechin, alpha-pinene and high amounts of hydrocarbons [6]. It is believed that the catechin fraction present in the rosemary extracts contributes to the inhibitive properties that act upon the alloy. *Rosmarinus officinalis* was evaluated to be an effective corrosion inhibitor on Al + 2.5 Mg alloy in 3% NaCl solution [7]. The inhibition properties of *R. officinalis* were studied by Yee [8] on aluminum, copper, iron and zinc in sodium chloride and sodium sulfate solutions. Cathodic inhibition was observed when the metal was polarized in sodium chloride solution.

🙋 Springer

Ouariachi et al. [9] reported on the inhibitory action of *R. officinalis* on C38 steel in 0.5 M H_2SO_4. Velázquez-González et al. [10] studied the corrosion inhibition effect of *R. officinalis* on carbon steel using extracts of acetone, hexane and methanol. The compounds performed effectively with high inhibition efficiency obtained from the hexane extract in the presence of flavonoids. Other researches by various authors confirm the excellent inhibition effect of *R. officinalis* on metallic alloys [11–15]. Vanillin derivative has been proven to be good inhibitor against metallic corrosion especially in combination with other compounds [16–21]. This research aims to study the synergistic effect of *R. officinalis* and 5-bromovanillin on the corrosion inhibition of 1018CS in 1 M HCl and H_2SO_4 solution.

Experimental Methods

Materials and Preparation

1018 carbon steel (1018CS) with a nominal composition as shown in Table 1 was the steel sample for the corrosion test. The steel in cylindrical form with dimensions of 1 cm length and 1 cm diameter after machining was abraded with silicon carbide papers (80, 320, 600, 800 and 1000 grits) before washing with distilled water and propanone, and kept in a desiccator for coupon analysis and potentiodynamic polarization test according to ASTM G1-03 (2011) [22]. 5-bromovanillin obtained from BOC Sciences, USA, and *R. officinalis* obtained from NOW Foods, USA, are the organic compounds to be assessed for their combined corrosion inhibiting properties. *Rosmarinus officinalis* is a golden, translucent, oily liquid with major compositions such as p-cymene (44.02%), linalool (20.5%), gamma-terpinene (16.62%), thymol (1.81%), beta-pinene (3.61%), alpha-pinene (2.83%) and eucalyptol (2.64%). It is also composed of monoterpenic hydrocarbons, oxygenated monoterpenes and sesquiterpene hydrocarbons [23]. It has a molar mass of 691.14 g/mol. 5-bromovanillin is a phenolic aldehyde organic compound with the molecular formula of $C_8H_8O_3$ and molar mass of 152.15 g/mol. It is the primary component of the extract of the vanilla bean and is used as a flavoring agent in foods, beverages and pharmaceuticals. Their combined admixture (ROSV) was prepared in molar concentrations of 2.96×10^{-3}, 5.93×10^{-2}, 8.89×10^{-2}, 1.19×10^{-2}, 1.48×10^{-2}, 1.78×1^{-2}, in 200 mL of 1 M HCl and H_2SO_4 solutions, prepared from analar grade of HCl acid (37%) and H_2SO_4 acid (98%) with deionized water.

Potentiodynamic Polarization Test

Polarization measurements were carried out at 30 °C using a three electrode system and glass cell containing 200 mL of the corrosive test solution at predetermined concentrations of ROSV with Digi-Ivy 2311 electrochemical workstation. Cylindrical 1018CS electrodes mounted in acrylic resin with an exposed surface area of 0.79 cm^2 were prepared according to ASTM G59-97 (2014) [24]. Polarization plots were obtained at a scan rate of 0.0015 V/s between potentials of −1.25 and +0.5 V according to ASTM G102-89 (2015) [25]. Platinum rod was used as the counter electrode and silver chloride electrode (Ag/AgCl) as the reference electrode. Corrosion current density (J_{cr}, A/cm^2) and corrosion potential (E_{cr}, V) values were obtained using the Tafel extrapolation method whereby the estimated corrosion current, I_{cr}, was obtained from the intercept of the two linear segments of the Tafel slope from the cathodic and anodic polarization plots [26, 27]. The corrosion rate, C_R (mm/year), was calculated from the mathematical relationship given below,

$$C_R = \frac{0.00327 \times J_{cr} \times E_{qv}}{d} \qquad (Eq\ 1)$$

where E_{qv} is the sample equivalent weight (g), 0.00327 is a constant for corrosion rate calculation [28] and d is the density (g/cm^3). The inhibition efficiency (η, %) was determined from the corrosion rate values according to Eq 2,

$$\eta_2 = 1 - \left[\frac{C_{R2}}{C_{R1}}\right] \times 100 \qquad (Eq\ 2)$$

C_{R1} and C_{R2} are the corrosion rates without and with ROSV compound. Polarization resistance, R_p (Ω), was calculated from Eq 3 given below,

$$R_p = 2.303 \frac{B_a B_c}{B_a + B_c} \left(\frac{1}{I_{cr}}\right) \qquad (Eq\ 3)$$

where B_a is the anodic Tafel slope and B_c is the cathodic Tafel slope, both are measured as (V/dec).

ATF-FTIR Spectroscopy and Optical Microscopy Characterization

ROSV/1 M HCl and H_2SO_4 solution (before and after the corrosion test) was exposed to specific range of infrared ray beams from Bruker Alpha FTIR spectrometer between wavelengths of 375 and 7500 cm^{-1} and resolution of

Table 1 Nominal (wt.%) composition of 1018CS

Element symbol	Mn	P	S	C	Fe
% composition (1018CSS)	0.8	0.04	0.05	0.16	98.95

0.9 cm^{-1}. The transmittance and reflectance of the infrared beams at various frequencies were decoded and transformed into an IR absorption plot consisting of spectra peaks. The spectral pattern was evaluated and equated to the theoretical IR absorption table to identify the functional groups involved in the corrosion inhibition reactions. Images of corroded and inhibited 1018CS surface morphology from optical microscopy were analyzed after weight loss measurement with Omax trinocular through the aid of ToupCam analytical software.

Weight Loss Measurement

Measured 1018CS steel coupons separately immersed in 200 mL of the dilute acid test solution for 240 h at 30°C were weighed every 24 h according to ASTM G31-72 (2004) [29]. Corrosion rate (C_R) is determined as follows,

$$C_R = \left[\frac{87.6\omega}{DAt}\right] \quad \text{(Eq 4)}$$

ω is the weight loss (g), D is the density (g/cm^3), A is the total surface area of the coupon (cm^2) and 87.6 is a constant for corrosion rate determination. t is the time (h). Inhibition efficiency (η) was determined from the mathematical relationship,

$$\eta = \left[\frac{\omega_1 - \omega_2}{\omega_1}\right] \times 100 \quad \text{(Eq 5)}$$

ω_1 and ω_2 are the weight loss of each steel coupon at specific ROSV concentrations. Surface coverage was determined from the relationship [30, 31]:

$$\theta = \left[1 - \frac{\omega_2}{\omega_1}\right] \quad \text{(Eq 6)}$$

where θ is the degree of ROSV compound, adsorbed per gram of the steel samples.

Results and Discussion

Potentiodynamic Polarization Studies

The anodic/cathodic polarization curves for the corrosion inhibition of ROSV on 1018CS in HCl and H$_2$SO$_4$ acid solution are shown in Figs. 1 and 2. Results of the polarization curves are presented in Table 2. Variation in corrosion rate for sample A at 0% ROSV and samples B–G (0.25–1.5% ROSV) in both acid solutions is due to the adsorption of ROSV compound on the steel's surface. The current peaks of the polarization curves in HCl solution (Fig. 1) decreased significantly with increase in ROSV concentration. Precipitation of ROSV molecules shifts the polarization curves in the anodic direction, as confirmed

from the corrosion potential values in Table 2. Changes in ROSV concentration has no significant influence on the cathodic Tafel slopes at all concentrations evaluated and hence on the hydrogen evolution and oxygen reduction reactions. The anodic Tafel value at 0% ROSV is due to the presence of surface oxides resulting from the slow electron transfer step [32, 33]. There is an increase in Tafel slope values after 0% ROSV, and it is due to changes in the electrode substrate, rate controlling step and influence of potential controlled conditions (i.e., high coverage by intermediates). The values show that addition of ROSV altered the oxidation electrochemical reactions, confirming the mechanism of inhibition to be probably as a result of surface coverage whereby ROSV inhibits the electrolytic transport and diffusion of corrosive anions (Cl$^-$ ions) to the carbon steel at the metal solution interface. This is further proven from the inhibition efficiency, whose values increased in proportion to ROSV concentration. At 0.25% ROSV, the inhibition efficiency is 52.45%, the value increased to 85.27% at 0.75% ROSV, after which the values remained above 90% till 1.5% ROSV.

1018CS at 0–0.75% ROSV (Fig. 2) was subject to severe anodic dissolution in H$_2$SO$_4$ solution. The corrosion rate significantly improved after 0.75% ROSV, but changes in corrosion rate values were marginal at 60% average till 1.5% ROSV and significantly lower than values obtained in HCl solution due to the high current density at the intercept between the anodic and cathodic polarization curves. The corrosion potential shifts in the cathodic direction of the potential domain after 0% ROSV due to release of excess electrons, thus slowing the anodic reaction and speeding up the cathodic process before shifting in the anodic direction from 0.75 to 1.5% ROSV. This observation is presented as a wide scatter in the polarization curve due to ROSV addition. The lower anodic Tafel slope values in H$_2$SO$_4$ in comparison with HCl show that 1018CS electrode is a strong electrocatalyst at high overpotentials in H$_2$SO$_4$. ROSV inhibition characteristics in the acid solution are probably through surface coverage and modification of the corrosive environment whereby reduction reactions are significantly influenced [34]. The differences in coverage of the steel surface by the adsorbed ROSV species in both acids is explained by the Langmuir, Frumkin, Freundlich and Temkin adsorption isotherms and is responsible for the corrosion rate values of 1018CS. The maximum change in corrosion potential of 1018CS in HCl solution is 42 mV, while in H$_2$SO$_4$ the change in corrosion potential is 52 mV; thus, ROSV is a mixed type inhibitor in both acid media.

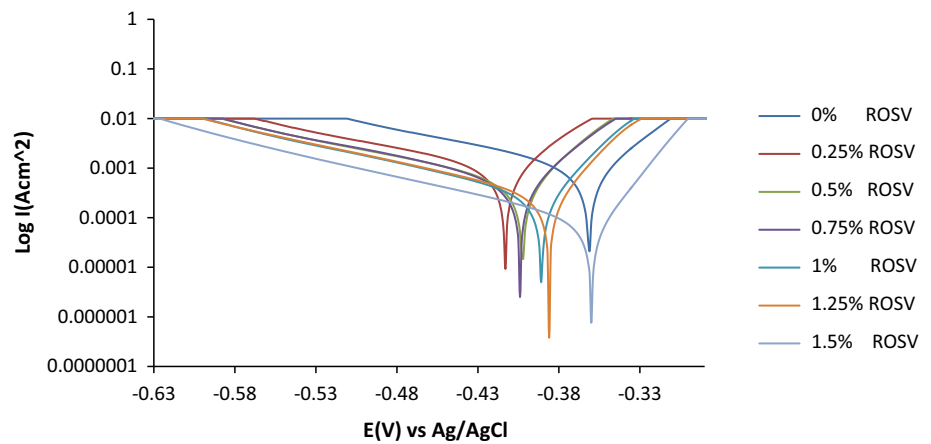ATF-FTIR Spectroscopy Analysis

Identification of the functional groups active in ROSV inhibition of 1018CS in HCl and H$_2$SO$_4$ acid solution was

Fig. 1 Potentiodynamic polarization curves for 1018CS in (0–1.5% ROSV) 1 M HCl
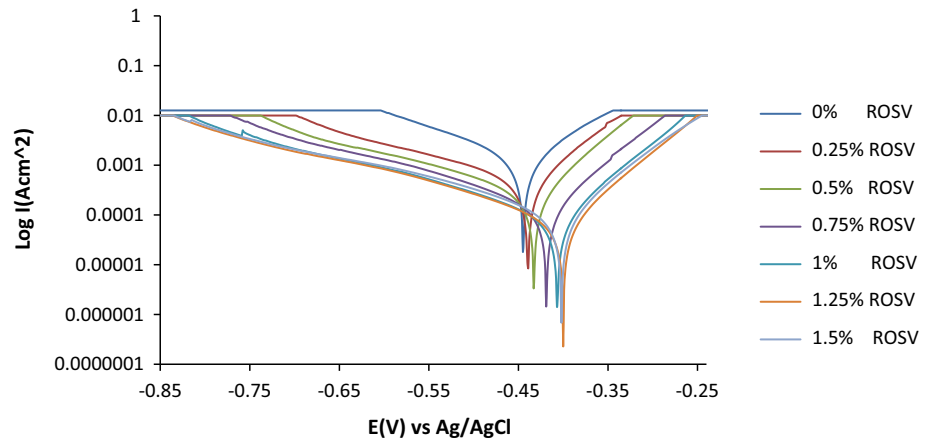
Fig. 2 Potentiodynamic polarization curves for 1018CS in (0–1.5% ROSV) 1 M HCl

Table 2 Potentiodynamic polarization data for 1018CS in 1 M HCl and H_2SO_4 (0–1.5% ROSV) acid solution

Sample	ROSV conc. (%)	ROSV conc. (M)	Corrosion rate (mm/y)	ROSV inhibition efficiency (%)	Corrosion current (A)	Corrosion current density (A/cm^2)	Corrosion potential (V)	Polarization resistance, R_p (Ω)	Cathodic Tafel slope, B_c (V/dec)	Anodic Tafel slope, B_a (V/dec)
HCl solution										
A	0	0	16.93	0	1.15E-03	1.46E-03	−0.445	34.76	−6.344	9.983
B	0.25	2.96E-06	8.05	52.45	5.48E-04	6.94E-04	−0.439	46.87	−5.058	14.150
C	0.5	5.93E-06	4.52	73.31	3.08E-04	3.89E-04	−0.433	83.50	−5.722	15.080
D	0.75	8.89E-06	2.49	85.27	1.70E-04	2.15E-04	−0.419	151.30	−6.451	16.420
E	1	1.19E-05	1.53	90.98	1.04E-04	1.32E-04	−0.407	247.20	−6.319	14.520
F	1.25	1.48E-05	1.26	92.57	8.57E-05	1.08E-04	−0.400	300.00	−6.329	14.890
G	1.5	1.78E-05	1.58	90.67	1.08E-04	1.36E-04	−0.402	238.80	−6.250	14.080
H_2SO_4 solution										
A	0	0	23.22	0	1.58E-03	2.00E-03	−0.361	16.25	−6.485	9.631
B	0.25	2.96E-06	22.09	4.89	1.50E-03	1.90E-03	−0.413	16.12	−6.241	11.506
C	0.5	5.93E-06	13.77	40.69	9.38E-04	1.19E-03	−0.402	27.40	−6.670	13.116
D	0.75	8.89E-06	12.86	44.60	8.76E-04	1.11E-03	−0.404	29.34	−6.980	11.430
E	1	1.19E-05	8.69	62.56	5.92E-04	7.49E-04	−0.391	45.72	−7.521	12.153
F	1.25	1.48E-05	8.44	63.64	5.75E-04	7.28E-04	−0.386	44.69	−7.367	11.087
G	1.5	1.78E-05	8.23	64.57	5.60E-04	7.09E-04	−0.360	142.50	−7.381	11.752

performed through ATF-FTIR spectroscopy and matched with the theoretical IR table [35, 36]. The IR spectra of 1 M HCl/ROSV and H_2SO_4/ROSV solution before and after the corrosion tests are shown in Figs. 3 and 4. The spectra diagram (Fig. 3) for ROSV in HCl before corrosion test shows peak configurations at some wavelength with intensities of 3350.43, 2921.81, 2855.86, 2169.15, 1634.86 and 1458.03 cm^{-1} which refers to N–H stretch (amines and amides), O–H stretch, H–bonded (alcohols and phenols), C–H stretch (alkanes), –C≡C– stretch (alkynes), N–H bend (amine), C–C stretch in-ring (aromatics) and N–O asymmetric stretch (nitro compounds). After the corrosion test, only the spectra peaks of 3331.26 and 1631.37 cm^{-1} remained as shown in the diagram due to chemisorption adsorption of the functional groups at other peaks. This is responsible for the strong electrochemical action of ROSV in HCl due to complete hydrolysis and ionization of the organic compound which formed a protective film on the carbon steel surface.

The electrochemical action of ROSV in H_2SO_4 (Fig. 4) contrasts its behavior in HCl solution. The spectra peaks before corrosion test consist of 3353, 2954.05–2852.30, 1460.74, 1376.96, 1168.40, 1052.35 and 721 cm^{-1} which

corresponds to O–H stretch, H–bonded (alcohols, phenols), N–H stretch (amines and amides), O–H stretch (carboxylic acids), C–H stretch (alkanes), C–C stretch in–ring (aromatics), C–H bend (alkanes), C–H rock (alkanes), C–O stretch (esters, ethers), C–H wag (alkyl halides) and C–N stretch (aliphatic amines). Studying the peaks after corrosion, there is no significant change in the wave number of the peaks but only a decrease in the peak intensity signifying limited adsorption of the functional groups of ROSV on 1018CS in H_2SO_4. This is probably responsible for the comparatively lower corrosion rate and inhibition efficiency values. While most of the spectra peaks for ROSV in HCl disappeared due to chemisorption as earlier explained, the spectra peaks in H_2SO_4. In HCl, several points of inhibitor/metal interaction can be deduced from the spectra peaks.

Weight Loss Measurement and Optical Microscopy Analysis

Data obtained for weight loss (ω), corrosion rate (C_R) and ROSV inhibition efficiency (ɲ) in 1 M HCl and H_2SO_4 acid media at 240 h are presented in Table 3. Figures 5a, b and

Fig. 3 IR spectra of ROSV compound in 1 M HCl solution before and after 1018CS corrosion test
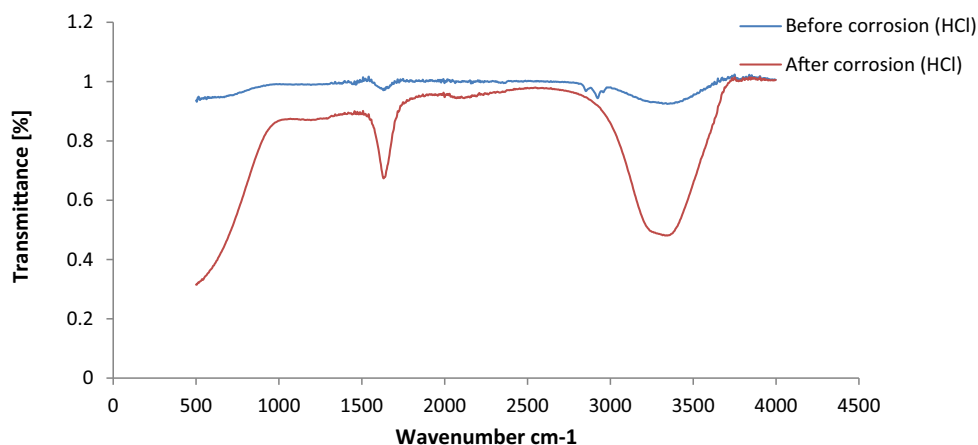
Fig. 4 IR spectra of ROSV compound in 1 M H_2SO_4 solution before and after 1018CS corrosion test

1036

J Fail. Anal. and Preven. (2017) 17:1031–1043
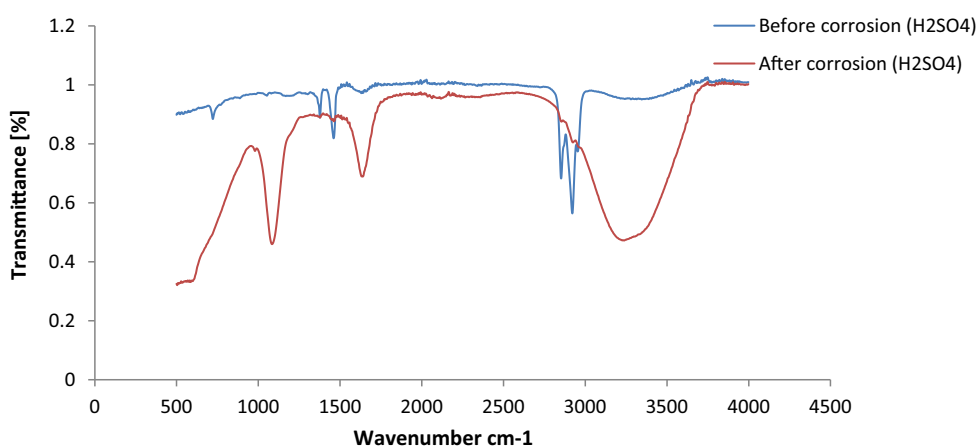
6a, b show the plot of 1018CS corrosion rate and ROSV inhibition efficiency versus exposure time in the acid solutions. Macroimages of the 1018CS before corrosion and after corrosion with and without ROSV effect are shown in Fig. 7a–c. Microanalytical images of 1018CS morphology before corrosion and after corrosion, without ROSV and in the presence of ROSV are shown in Figs. 8a, b, 9a, b, 10a, b, 11a, b, and 12a, b at mag. ×40 and ×100. At 0% ROSV (Figs. 5a and 6a), 1018CS undergo severe anodic dissolution in HCl and H_2SO_4 acids due to the presence and electrochemical action of SO_4^{2-} and Cl^- ions resulting in the formation of porous oxides on the steel surface (Figs. 9a and 10b). Continuous deterioration and oxide formation lead to the formation of pores and channels within the oxide layer which further accelerates the corrosion of the steel (Fig. 7c) [37]. The corrosion rate at 0% ROSV in H_2SO_4 declined progressively with time until 144 h; wherewith, it remained generally constant till 240 h while the corrosion rate in HCl solution alternated at high values throughout the exposure hours. Values for H_2SO_4 are significantly higher than in HCl due to the ability of H_2SO_4 to completely ionize in the solution releasing two protons which reacts strongly with 1018CS surface compared to HCl which releases one proton. Transition from active deterioration of the steel surface to the passive state in the presence of ROSV (Fig. 12a and b) was gradual in H_2SO_4 due to inability of ROSV adsorption to sufficiently inhibit 1018CS corrosion until 1–1.25% ROSV (Fig. 6b); wherewith, the inhibition efficiency stabilized at an average value of 62.4%. In HCl, adsorption of ROSV through electrostatic attraction with the ionized valence atoms on the carbon steel surface results in effective corrosion inhibition from 0.25 to 1.5% ROSV (Fig. 6a). More ROSV molecules are adsorbed on the steel surface at higher concentrations, leading to greater surface coverage [38]. This is due to the electrochemical reactions of ROSV within HCl solution which results in the formation of a protective, adherent film that sufficiently hindered the access of Cl^- ions to the metal surface. Its molecules interact with the redox cells, retarding the electrochemical process. ROSV protonates more strongly in HCl than H_2SO_4 releasing more electrons from its molecules; this phenomenon increases the reactivity of the ROSV enabling strong adsorption with the steel surface.

Adsorption Isotherm

The corrosion inhibition and adsorption of ROSV compounds over 1018CS surface in the acid media is responsible for the reaction rate of the steel as a result of the strong interaction between the steel surface and the pi-electrons within the heteroatoms of the inhibiting compound [39]. Organic adsorption from aqueous solution is relatively complex and depends on the property of the interfacial region between the steel and acid solution. Due to the solvated nature of the interfacial region, the electrochemical adsorption can be viewed as a replacement reaction of water molecules in the adsorbed layer by ROSV molecules within the bulk acid solution [40, 41]. A number of adsorption models have been previously applied to assess experimental results [42]; however, in this research Langmuir, Freundlich and Temkin adsorption isotherm produced the best fit as shown in Figs. 13, 14, 15, 16, 17, and 18 according to the following equations,

Table 3 Data from weight loss analysis at 240 h for 1018CS in 1 M HCl and H_2SO_4 solution (0–1.5% ROSV)

Samples	Weight loss (g)	ROSV concentration (%)	ROSV concentration (M)	Corrosion rate (mm/year)	ROSV inhibition efficiency (%)
HCl					
A	4.211	0	0	0.034	0
B	1.016	0.25	2.96E−06	0.008	75.87
C	0.553	0.5	5.93E−06	0.004	86.86
D	0.346	0.75	8.89E−06	0.003	91.78
E	0.267	1	1.19E−05	0.002	93.66
F	0.253	1.25	1.48E−05	0.002	94.00
G	0.202	1.5	1.78E−05	0.002	95.20
H_2SO_4					
A	5.753	0	0	0.047	0
B	5.100	0.25	2.96E−06	0.041	12.93
C	3.146	0.5	5.93E−06	0.026	45.32
D	2.747	0.75	8.89E−06	0.022	52.25
E	2.293	1	1.19E−05	0.019	60.14
F	2.157	1.25	1.48E−05	0.018	62.50
G	2.040	1.5	1.78E−05	0.017	64.55

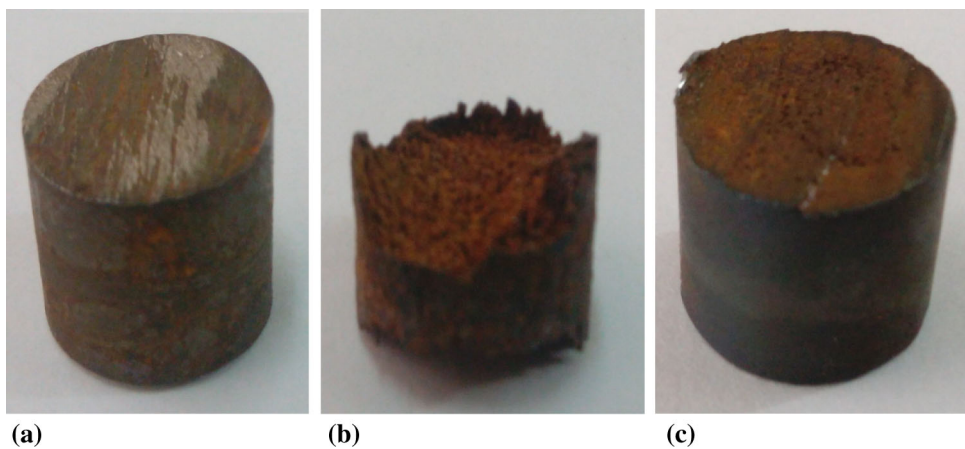**Fig. 5** Plot of (**a**) 1018CS corrosion rate vs. exposure time in HCl (**b**) 1018CS corrosion rate vs. exposure time in H₂SO₄

(a)   (b)
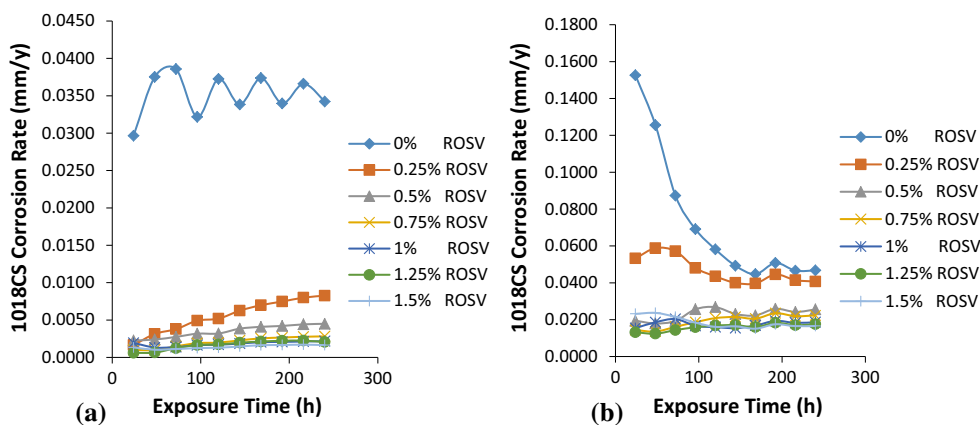
Fig. 6 ROSV inhibition efficiency vs. exposure time at 0–1.5% ROSV concentration (**a**) in 1 M HCl, (**b**) in 1 M H₂SO₄

(a)   (b)
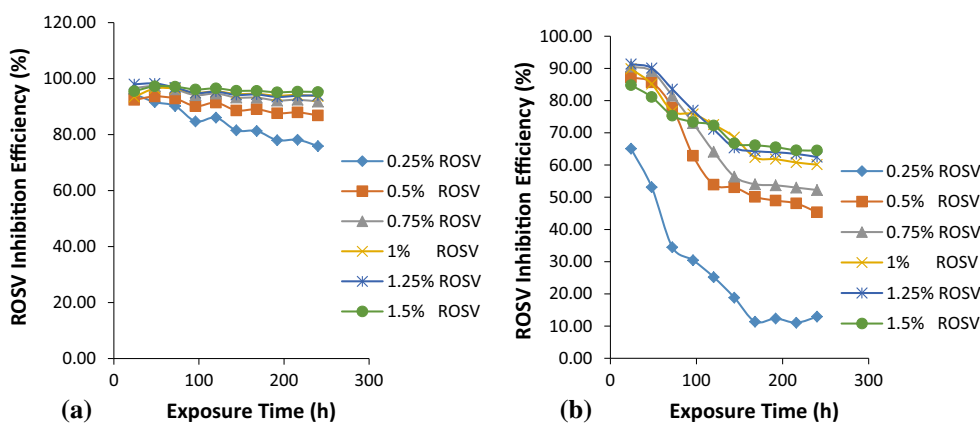
Fig. 7 Macroimages of 1018CS (**a**) before corrosion, (**b**) after corrosion without ROSV and (**c**) after corrosion with ROSV


(a)   (b)   (c)

$$\theta = \left[\frac{K_{ads}C_{ROSV}}{1 + K_{ads}C_{ROSV}} \right] \qquad \text{(Eq 7)}$$

where θ is the degree of ROSV surface coverage on 1018CS, C_{ROSV} is ROSV concentration and K_{ads} is the equilibrium constant of the adsorption mechanism. The plots of $\frac{C_{ROSV}}{\theta}$ versus C_{ROSV} for ROSV adsorption in HCl showed linearity in agreement with Langmuir adsorption

isotherm (Fig. 13) with a correlation coefficient of 0.9999. In H₂SO₄, the plots (Fig. 14) deviated from ideal Langmuir model with a correlation coefficient of 0.3561. Langmuir isotherm suggests single layer adsorption, adsorption occurs at definite number of reaction sites, all adsorptions are identical and equivalent and no lateral interaction between the adsorbed molecules [43].
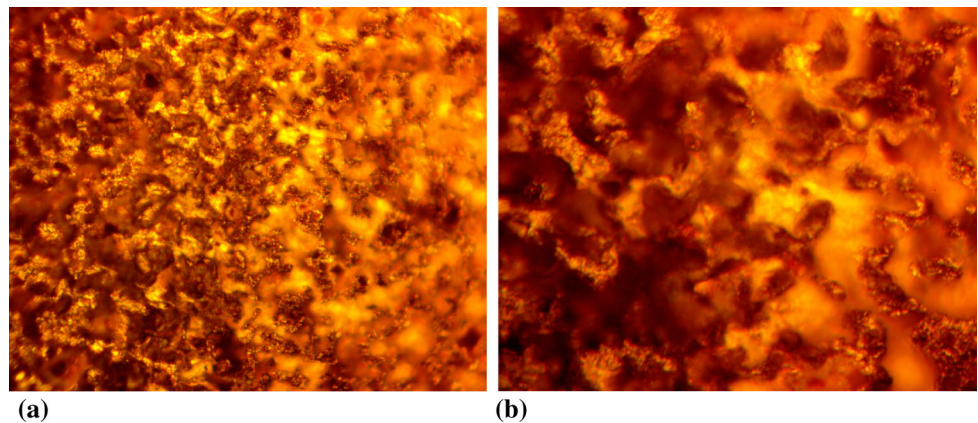
Fig. 8 Microanalytical image of 1018CS before corrosion (**a**) mag. ×40, (**b**) mag. ×100

(**a**)   (**b**)
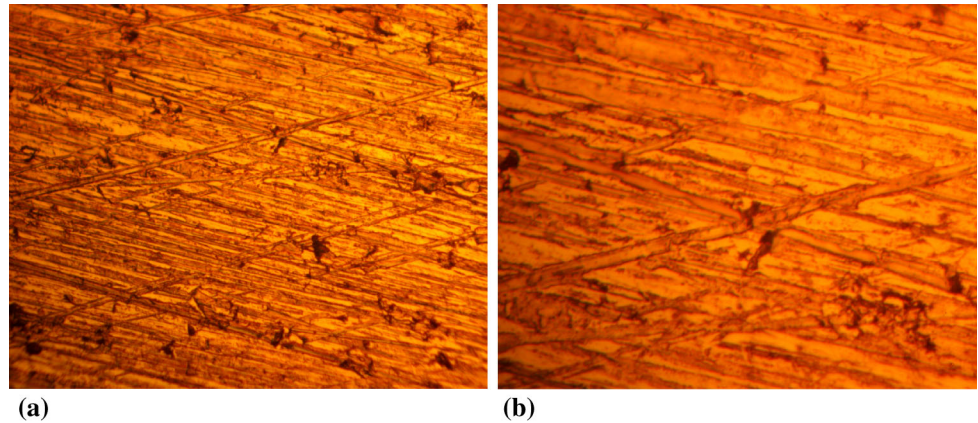
Fig. 9 Microanalytical image of 1018CS after corrosion in HCl without ROSV (**a**) mag. ×40, (**b**) mag. ×100

(**a**)   (**b**)
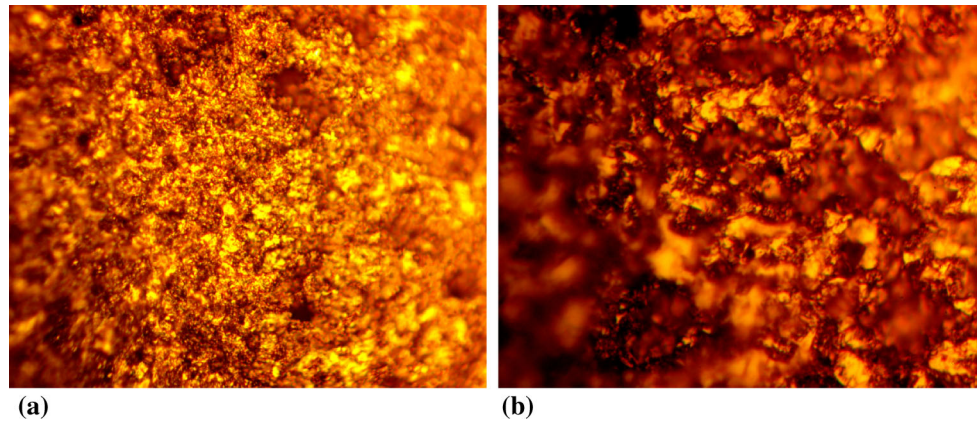
Fig. 10 Microanalytical image of 1018CS after corrosion in H₂SO₄ without ROSV (**a**) mag. ×40, (**b**) mag. ×100

(**a**)   (**b**)

$$\theta = KC^n \tag{Eq 8}$$

$$\log \theta = n \log C + \log K_{ads} \tag{Eq 9}$$

where n is a constant depending on the characteristics of the adsorbed molecule and K_{ads} is the adsorption–desorption equilibrium constant denoting the strength of interaction in the adsorbed layer. The Freundlich isotherm states that adsorbed molecules interact and influence further adsorption through repulsion or attraction of molecules. The amount adsorbed is the total of adsorption on all sites, with the more reactive sites being first occupied, until adsorption energy is exponentially decreased upon the completion of adsorption process [44, 45]. The correlation coefficient for Freundlich isotherm plot (Fig. 15) for ROSV adsorption in HCl is 0.7549, while in H₂SO₄ (Fig. 16) it is 0.7668.
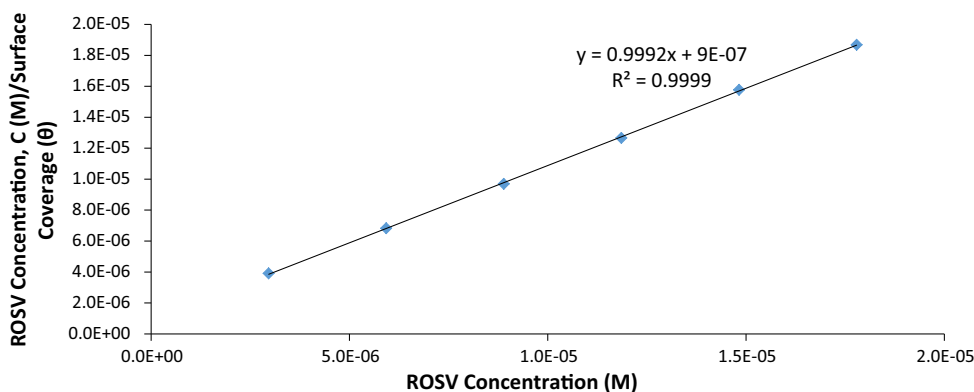
Fig. 11 Microanalytical image of 1018CS after corrosion in HCl with ROSV (**a**) mag. ×40, (**b**) mag. ×100

(a)   **(b)**
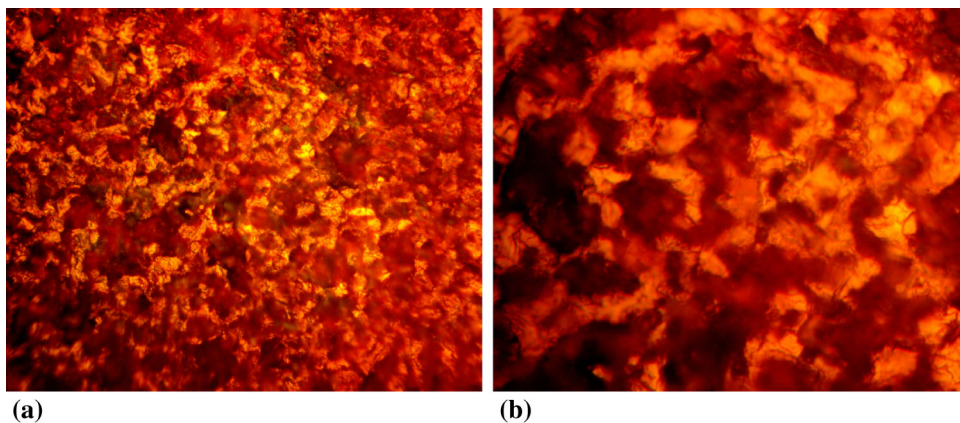
Fig. 12 Microanalytical image of 1018CS after corrosion in H₂SO₄ with ROSV (**a**) mag. ×40, (**b**) mag. ×100

(a)   **(b)**
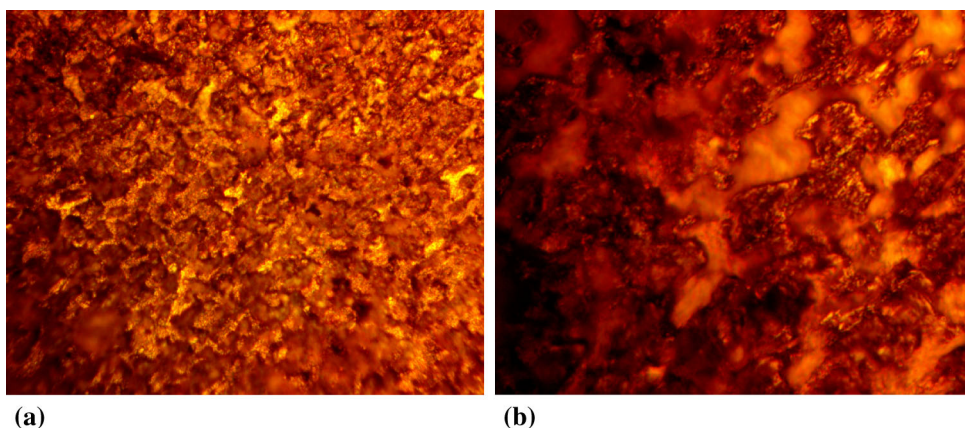
Fig. 13 Langmuir plot of $\frac{C}{\theta}$ vs. ROSV concentration in 1 M HCl

$$qe \ = \ B \ln(A + Ce) \qquad \text{(Eq 10)}$$

$$\text{Where } B \ = RT/b \qquad \text{(Eq 11)}$$

where A is Temkin isotherm constant (L/g), b is the Temkin constant related to heat of adsorption, T is the temperature (K), R is the gas constant (8.314, J/mol K) and Ce is the concentration of adsorbate. B is the Temkin constant related to heat of sorption (J/mol). The Temkin isotherm assumes the heat of adsorption decreases linearly with increase in surface coverage. It is characterized by a

uniform distribution of binding energies, taking into account the indirect interactions of adsorbate–adsorbate molecules on adsorption isotherm [46]. The Temkin isotherm plot for ROSV in HCl (Fig. 17) had a correlation coefficient of 0.9380, while in H₂SO₄ it is 0.9359 (Fig. 18).
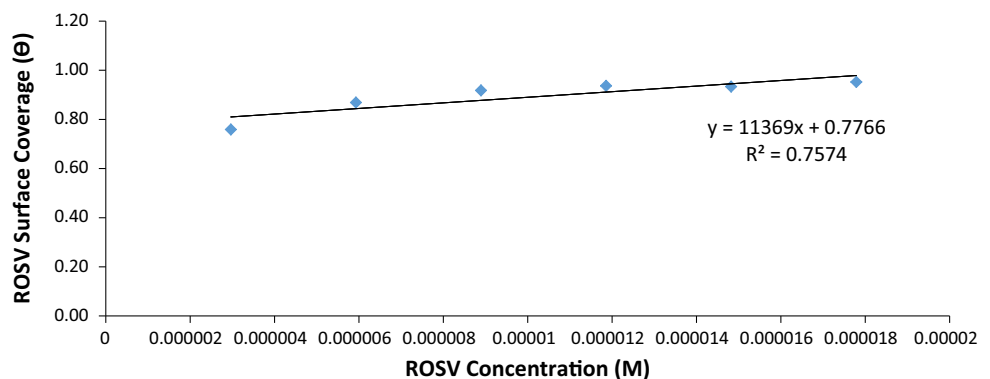
Thermodynamics of the Corrosion Process

The strength of adsorption of ROSV on 1018CS can be determined from the thermodynamics of the inhibition
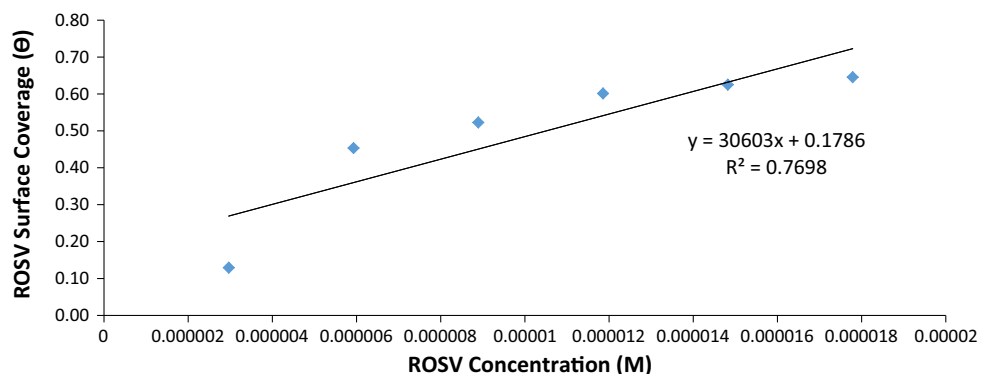
Fig. 14 Langmuir plot of $\frac{C}{\theta}$ vs. ROSV concentration in 1 M H_2SO_4
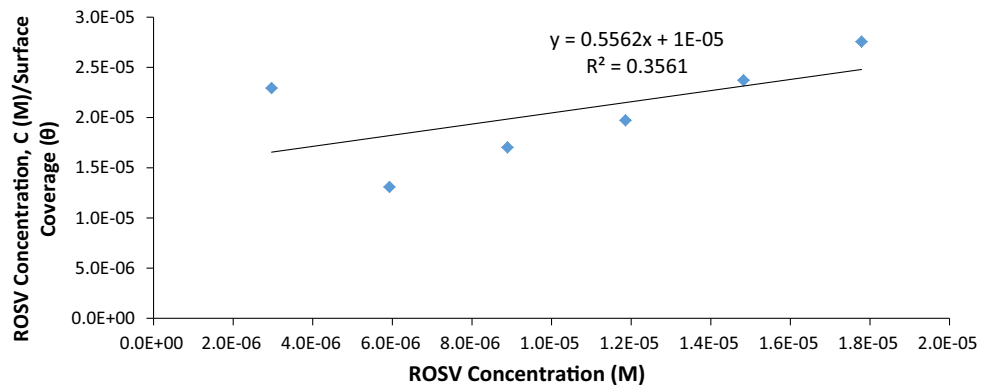
Fig. 15 Freundlich isotherm plot of ROSV surface coverage (θ) vs. ROSV concentration in HCl solution

Fig. 16 Freundlich isotherm plot of ROSV surface coverage (θ) vs. ROSV concentration in H_2SO_4 solution

mechanism. Calculated results of Gibbs free energy (ΔG_{ads}^{o}) for the adsorption process shown in Tables 4 and 5 were evaluated from the relationship [47].

$$\Delta G_{ads} = -2.303RT \log[55.5 K_{ads}] \qquad \text{(Eq 12)}$$

where 55.5 is the molar concentration of water in the solution, R is the universal gas constant, T is the absolute temperature and K_{ads} is the equilibrium constant of adsorption. K_{ads} is related to surface coverage (θ) from the Langmuir equation.

The presence of flaws, impurities, inclusions, etc., on the steel surface significantly affect the values of ΔG_{ads}^{o} with changes in surface coverage value of ROSV [48]. The amount of cations passed into the solution is related to the extent of coverage of ROSV inhibitor over the 1018CS surface. The negative values of ΔG_{ads}^{o} show the spontaneity and stability of the adsorption mechanism. The highest and lowest values of ΔG_{ads}^{o} in HCl are value obtained is −44.75 KJ/mol at 0.25% ROSV and −44.05 KJ/mol at 1.25% ROSV. The values align with chemisorption adsorption mechanism involving charge sharing or transfer between the inhibitor cations and the valence electrons of the metal forming a coordinate covalent bond [49, 50]. In H_2SO_4, the values are −39.31 KJ/mol at 0.5% ROSV and −36.77 KJ/mol at 0.25% ROSV. These values in H_2SO_4 are consistent with physiochemical adsorption mechanism.

Fig. 17 Temkin isotherm plot of ROSV surface coverage (θ) vs. log ROSV concentration in HCl

$$y = 0.2464x + 2.1404$$
$$R^2 = 0.9380$$
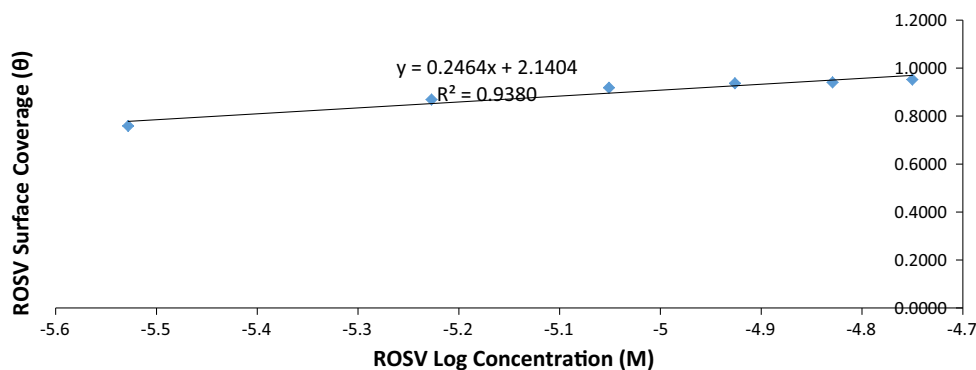
Fig. 18 Temkin isotherm plot of ROSV surface coverage (θ) vs. log ROSV concentration in H$_2$SO$_4$

$$y = 0.6503x + 3.7815$$
$$R^2 = 0.9359$$
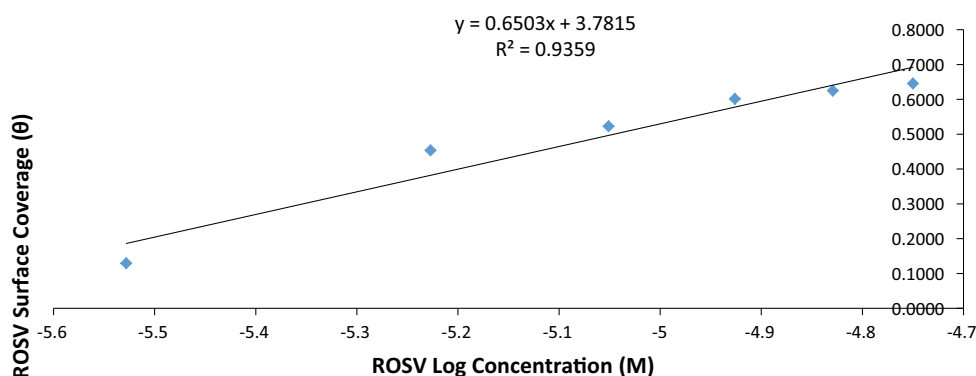
Table 4 Data for Gibbs free energy (ΔG^o_{ads}), surface coverage (θ) and equilibrium constant of adsorption (K_{ads}) for ROSV adsorption on 1018CS in HCl

Samples	ROSV concentration (M)	Surface coverage (θ)	Equilibrium constant of adsorption (K)	Gibbs free energy, ΔG (KJ/mol)
A	0	0	0	0
B	2.965E-06	0.759	1060615.0	−44.33
C	5.929E-06	0.869	1115179.4	−44.46
D	8.894E-06	0.918	1255603.0	−44.75
E	1.186E-05	0.937	1246167.1	−44.73
F	1.482E-05	0.933	944965.6	−44.05
G	1.779E-05	0.952	1115758.9	−44.46

Table 5 Data for Gibbs free energy (ΔG^o_{ads}), surface coverage (θ) and equilibrium constant of adsorption (K_{ads}) for ROSV adsorption on 1018CS in H$_2$SO$_4$

Samples	ROSV concentration (M)	Surface coverage (θ)	Equilibrium constant of adsorption (K)	Gibbs free energy, ΔG (KJ/mol)
A	0	0	0	0
B	2.965E-06	0.129	50077.2	−36.77
C	5.929E-06	0.453	139782.6	−39.31
D	8.894E-06	0.523	123039.5	−39.00
E	1.186E-05	0.601	127217.9	−39.08
F	1.482E-05	0.625	112451.2	−38.77
G	1.779E-05	0.645	102353.5	−38.54

Conclusion

ROSV effectively inhibited the corrosion and surface deterioration of 1018 carbon steel in dilute HCl acid solution but marginally inhibited in H_2SO_4. The organic compound chemisorbed onto the carbon steel in HCl, passivating it through identified functional groups in the compound from ATF-FTIR spectroscopy analysis. Physiochemical interaction was observed in H_2SO_4 solution resulting in significant surface deterioration of the carbon steel. The comparatively lower anodic Tafel slope values in H_2SO_4 show that 1018CS electrode is a strong electrocatalyst at high overpotentials. ROSV had no direct influence on the cathodic Tafel slopes in both acids at all concentrations. Changes in the anodic Tafel slope values in HCl were due to changes in the electrode substrate, rate controlling step and influence of potential controlled conditions due to surface coverage whereby ROSV inhibits the electrolytic transport and diffusion of corrosive anions. In both acids, inhibition efficiency was proportional to inhibitor concentration and the inhibition property of the compound was determined to be mixed type inhibitor.

References

1. E.S. Ferreira, C. Giacomelli, F.C. Giacomelli, A. Spinelli, Evaluation of the inhibitor effect of L-ascorbic acid on the corrosion of mild steel. Mater. Chem. Phys. **83**, 129–134 (2004)
2. M.A. Amin, S.S.A. El-Rehim, E.E.F. El-Sherbini, R.S. Bayoumy, The inhibition of low carbon steel corrosion in hydrochloric acid solutions by succinic acid: Part I: weight loss, polarization, EIS, PZC, EDX and SEM studies. Electrochim. Acta **52**, 3588–3600 (2007)
3. A. Bouyanzer, B. Hammouti, L. Majidi, Pennyroyal oil from Mentha pulegium as corrosion inhibitor for steel in 1 M HCl. Mater. Lett. **60**, 2840–2843 (2006)
4. P.B. Raja, M.G. Sethuraman, Natural products as corrosion inhibitor for metals in corrosive media—a review. Mater. Lett. **62**, 113–116 (2008)
5. A.A. Rahim, E. Rocca, J. Steinmetz, M.J. Kassim, Inhibitive action of mangrove tannins and phosphoric acid on pre-rusted steel via electrochemical methods. Corros. Sci. **50**, 1546–1550 (2008)
6. J.C. Chalchat, R.P. Garry, A. Michet, B. Benjilali, J.L. Chabart, Essential oils of Rosemary (Rosmarinus officinalis L.). The chemical composition of oils of various origins (Morocco, Spain, France). J. Essent. Oil Res. **5**(6), 613–618 (1993)
7. A.Y. El-Etre, Natural honey as corrosion inhibitor for metals and alloys. I. Copper in neutral aqueous solution. Corros. Sci. **40**(11), 1845–1850 (1998)
8. Y.J. Yee, Green inhibitors for corrosion control: a study on the inhibitive effects of extracts of honey and Rosmarinus officinalis L. (Rosemary), M.S. thesis, University of Manchester, Institute of Science and Technology, 2004
9. E. El Ouariachi, J. Paolini, M. Bouklah, A. Elidrissi, A. Bouyanzer, B. Hammouti, J-M. Desjobert, J. Costa, Adsorption properties of Rosmarinus officinalis oil as green corrosion inhibitors on C38 steel in 0.5 M H_2SO_4. Acta Metall. Sinica **23**(1), 13–20 (2010)
10. M.A. Velázquez-González, J.G. Gonzalez-Rodriguez, M.G. Valladares-Cisneros, I.A. Hermoso-Diaz, Use of Rosmarinus officinalis as green corrosion inhibitor for carbon steel in acid medium. Am. J. Anal. Chem. **5**, 55–64 (2014)
11. A.S. Fouda, A.M. Nofal, G.Y. El-Ewady, A.S. Abousalem, Eco-friendly impact of Rosmarinus officinalis as corrosion inhibitor for carbon steel in hydrochloric acid solutions. Der Pharma Chem. **7**(5), 183–197 (2015)
12. M. Bendahou, M. Benabdellah, B. Hammouti, A study of rosemary oil as a green corrosion inhibitor for steel in 2 M H_3PO_4. Pigment Resin Technol. **35**(2), 95–100 (2006)
13. S.A. Ćatić, E.B. Obralić, A. Bratovčić, Rosemary as ecologically acceptable corrosion inhibitor of steel. Bull. Chem. Technol. Bosnia Herzeg. **46**, 47–50 (2016)
14. R.T. Loto, E. Oghenerukewe, Inhibition studies of Rosmarinus officinalis on the pitting corrosion resistance 439LL ferritic stainless steel in dilute sulphuric acid. Orient. J. Chem. **32**(5), 2813–2832 (2016)
15. R.T. Loto, R.O. Loto, O.O. Joseph, I. Akinwumi, Electrochemical studies of the corrosion inhibition property of Rosmarinus officinalis on mild steel in dilute sulphuric acid. J. Chem. Pharm. Res. **7**(7), 105–116 (2015)
16. A.Y. El-Etre, Inhibition of acid corrosion of aluminum using vanillin. Corros. Sci. **43**(6), 1031–1039 (2001)
17. S.M. Tawfik, N.A. Negm, Vanillin-derived non-ionic surfactants as green corrosion inhibitors for carbon steel in acidic environments. Res. Chem. Intermed. **42**, 3579–3607 (2016)
18. M. Shahidi, E. Sasaei, M. Ganjehkaviri, M.R. Gholamhosseinzadeh, Investigation of the effect of vanillin as a green corrosion inhibitor for stainless steel using electrochemical techniques. J. Phys. Theor. Chem. **9**(3), 149–161 (2012)
19. R.T. Loto, O. Tobilola, Corrosion inhibition properties of the synergistic effect of 4-hydroxy-3-methoxybenzaldehyde and hexadecyltrimethylammoniumbromide on mild steel in dilute acid solutions. J. King Saud Univ. Eng. Sci. (2016). doi: Ĉ10.1016/j.jksues.2016.10.001
20. R.T. Loto, Study of the synergistic effect of 2-methoxy-4-formylphenol and sodium molybdenum oxide on the corrosion inhibition of 3CR12 ferritic steel in dilute sulphuric acid. Results Phys. **7**, 769–776 (2017)
21. R.T. Loto, Corrosion inhibition studies of the combined admixture of 1,3-diphenyl-2-thiourea and 4-hydroxy-3-methoxybenzaldehyde on mild steel in dilute acid media. Rev. Colomb. Quim. **46**(1), 20–32 (2017)
22. ASTM G1 - 03(2011) Standard Practice for Preparing, Cleaning, and Evaluating Corrosion Test Specimens. Ĉhttp://www.astm.org/Standards/G1. Retrieved 30 May 2016
23. M.M. Ozcan, J.C. Chalchat, Chemical composition and antifungal activity of rosemary (Rosmarinus officinalis L.) oil from Turkey. Int. J. Food Sci. Nutr. **59**(7–8), 691–698 (2008)
24. ASTM G59 - 97(2014) Standard Test Method for Conducting Potentiodynamic Polarization Resistance Measurements. Ĉhttp://www.astm.org/Standards/G31. Retrieved 30 May 2016
25. ASTM G102 - 89(2015) e1. Standard Practice for Calculation of Corrosion Rates and Related Information from Electrochemical Measurements. http://www.astm.org/Standards/G31. Retrieved 30 May 2016
26. Ĉhttp://www.che.sc.edu/faculty/popov/drbnp/ECHE789b/Corrosion%20Measurements.pdf. Retrieved 06 April 2017
27. http://www.ecochemie.nl/download/Applicationnotes/Autolab_Application_Note_COR02.pdf. Retrieved 06 April 2017

28. Y. Choi, S. Nesic, S. Ling, Effect of H_2S on the CO_2 corrosion of carbon steel in acidic solutions. Electrochim. Acta **56**, 1752–1760 (2011)
29. ASTM G31 - 72(2004) Standard Practice for Laboratory Immersion Corrosion Testing of Metals. Ćhttps://www.astm.org/DATABASE.CART/HISTORICAL/G31-72R04.htm. Retrieved 06 April 2017
30. H.U. Schutt, R.J. Horvath, *Crude column overhead corrosion problem caused by oxidized sulfur species* (NACE, Houston, 1987)
31. M.J. Schofield, *Plant Engineer's Reference Book* (Elsevier, Amsterdam, 2003)
32. J.O. Bockris, D. Drazic, A.R. Despic, The electrode kinetics of the deposition and dissolution of iron. Electrochim. Acta **4**, 325–361 (1961)
33. J.O. Bockris, H. Kita, Analysis of galvanostatic transients and application to the iron electrode reaction. J. Electrochem. Soc. **108**(7), 676–685 (1961)
34. K. Kinoshita, *Electrochemical Oxygen Technology* (Wiley, New York, 1992), p. 87
35. Table of Characteristic IR Absorptions. Ćhttp://orgchem.colorado.edu/Spectroscopy/specttutor/irchart.pdf. Retrieved 12 Jan 2017
36. S. George, *Infrared and Raman Characteristic Group Frequencies: Tables and Charts* (Wiley, New York, 2004)
37. M.A. Deyab, Effect of cationic surfactant and inorganic anions on the electrochemical behaviour of carbon steel in formation water. Corros. Sci. **49**, 2315–2328 (2007)
38. V.S. Rao, L.K. Singhal, Corrosion behavior and passive film chemistry of 216L stainless steel in sulphuric acid. J. Mater. Sci. **44**(9), 2327–2333 (2009)
39. J. Zhu, Th Hartung, D. Tegtmeyer, H. Baltruschat, J. Heitbaum, The electrochemical reactivity of toluene at porous Pt electrodes. J. Electroanal. Chem. **24**, 273–286 (1988)
40. K. Shimazu, H. Kita, Hydrogenation of 1,3-butadiene on Pd in sulfuric acid solution: II. Adsorbed hydrogen species. J. Catal. **83**, 407–414 (1983)
41. S. Trasatti, Acquisition and analysis of fundamental parameters in the adsorption of organic substances at electrodes. J. Electroanal. Chem. **53**, 335–363 (1974)
42. R. Guidelli, in *Adsorption of Molecules at Metal Electrodes*, ed. by J. Lip Kowski, P.N. Ross (VCH Publishers, lnc, New York, 1992), p. 1
43. S. Arivoli, K. Kalpana, R. Sudha, T. Rajachandrasekar, Comparative study on the adsorption kinetics and thermodynamics of metal ions onto acid activated low cost carbon. Eur. J. Chem. **4**(4), 238–254 (2007)
44. K.S. Ashish, M.A. Quraishi, Investigation of the effect of disulfiram on corrosion of mild steel in hydrochloric acid solution. Corros. Sci. **53**(4), 1288–1297 (2011)
45. J. Zeldowitsch, Adsorption site energy distribution. Acta Phys. Chim. URSS **1**, 961–973 (1934)
46. C. Aharoni, M. Ungarish, Kinetics of activated chemisorption. Part 2. Theoretical models. J. Chem. Soc. Faraday Trans. **73**, 456–464 (1977)
47. P. Lowmunkhong, D. Ungthararak, P. Sutthivaiyakit, Tryptamine as a corrosion inhibitor of mild steel in hydrochloric acid solution. Corros. Sci. **52**, 30–36 (2010)
48. O.K. Abiola, J.O.E. Otaigbe, Adsorption behaviour of 1-phenyl-3-methylpyrazol-5-one on mild steel from HCl solution. Int. J. Electrochem. Sci. **3**, 191–198 (2008)
49. M. Bouklah, B. Hammouti, M. Lagrene, F. Bentiss, Thermodynamic properties of 2, 5-bis(4-methoxyphenyl)-1, 3, 4-oxadiazole as a corrosion inhibitor for mild steel in normal sulfuric acid medium. Corros. Sci. **48**(9), 2831–2841 (2006)
50. R.T. Loto, Electrochemical analysis of the corrosion inhibition properties of 4-hydroxy-3-methoxybenzaldehyde on low carbon steel in dilute acid media. Cogent Eng. (2016). doi:Ć10.1080/23311916.2016.1242107